ACS OMEGA

http://pubs.acs.org/journal/acsodf

Article

Nanosized Hexagonal Boron Nitride and Polyethylene Glycol-Filled Leathers for Applications Demanding High Thermal Insulation and Impact Resistance

Arya P Bhasi, Nithiya Hanna Wilson, and Thanikaivelan Palanisamy*

Cite This: *ACS Omega* 2022, 7, 45120−45128

Read Online

ACCESS | Metrics & More | Article Recommendations | Supporting Information

ABSTRACT: Leather is a niche material used for upholsteries, gloves, and garments due to its high durability, flexibility, and softness properties. The inclusion of nanoparticles in the leather matrix provides multifunctionality for high-performance applications. Herein, we synthesized hexagonal boron nitride (h-BN) nanoparticles via a single-step hydrothermal synthesis and treated the leather after dispersing in polyethylene glycol (PEG) to yield h-BN/PEG-treated leathers. Atomic force microscopy and high-resolution transmission electron microscopy analysis ascertained the particle size of 30−50 nm for as-synthesized h-BN nanoparticles. h-BN nanoparticles along with PEG were successfully incorporated into the leather matrix, and this was confirmed by surface and morphological studies using field emission scanning electron microscopy/energy-dispersive X-ray analysis and Fourier transformed infrared spectroscopy. Leathers treated with h-BN/PEG were studied for insulation against heat and cold, and the results displayed improved thermal insulation properties compared to the control leathers. The dynamic mechanical analysis of control and treated leathers demonstrated higher storage modulus, loss modulus, and tan δ values for h-BN/PEG-treated leathers, signifying an increased energy absorption and dissipation potential, which was further ascertained by the low-velocity drop-weight impact resistance test. Thus, the results of this study open up new prospects for h-BN/PEG-treated leathers in strategic applications demanding high thermal insulation and impact resistance properties.

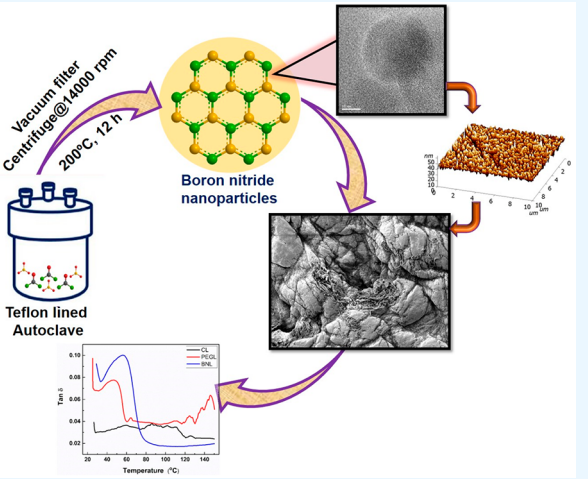

INTRODUCTION

Two-dimensional nanomaterials have achieved greater scientific interest over recent years due to their tunable optical, electrical, chemical, mechanical, magnetic, and thermal properties.[1] 2D nanomaterials, consisting of few-layered structures of graphene, hexagonal boron nitride (h-BN), and transition metal dichalcogenides, possess distinct properties dependent on different directions in their lattice structure and offer a wide range of applications. 2D inorganic compounds such as transitional metal carbides (MXenes) and functionalized boron nitride nanoparticles are used as nanofillers for improving the functional properties of the polymeric materials such as mechanical strength and fire retardancy.[2−4]

Hexagonal boron nitride, known as white graphene, is the structural analogue of graphene with alternate B−N bonds substituting the C−C bonds.[5] The intralayer σ bonds and interlayer van der Waals forces of h-BN are comparable to those of graphene and are in consonance with its thermally conductive, mechanically strong, and lubricating nature.[6] h-BN is chemically inert with low dielectric constant,[7] high thermal conductivity,[8] high electrical resistance,[9] low toxicity,[10] and photoluminescence in the UV range.[11] Due to its oxidation resistance and high-temperature stability, boron nitride nanoparticles are used as chemical-resistant coatings for metals.[12] h-BN nanoparticles are used to reinforce the polymer composites and alloys for increased thermal conductivity and improved mechanical properties.[13] Deep-UV absorbance of h-BN nanoparticles offers application in optoelectronics as well as sensors.[14] The energy-harvesting ability of BN nanostructures was achieved by their piezoelectric properties.[15]

Polyethylene glycols (PEGs) are hydrophilic polymers employed as viscosity modifiers, binders, lubricants, and surfactants with significant applications in biomedical fields as well as industries. It is a non-Newtonian fluid and is used as a dispersion medium in shear-thickening fluids (STFs). STFs

Received: August 29, 2022
Accepted: November 18, 2022
Published: December 1, 2022

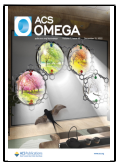

https://doi.org/10.1021/acsomega.2c05567
ACS Omega 2022, 7, 45120−45128

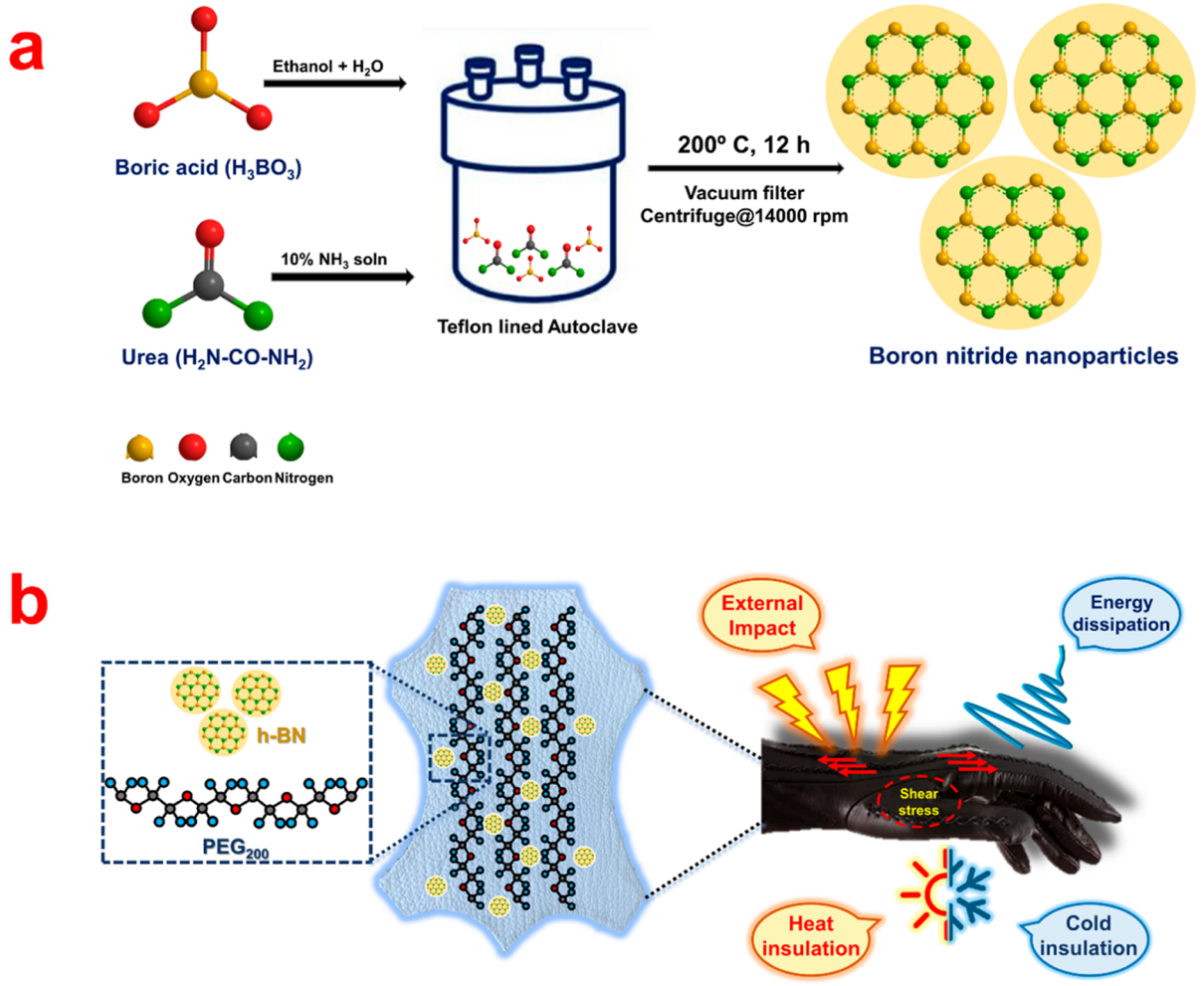

Figure 1. (a) Schematic representation of the h-BN nanoparticles synthesis. (b) Schematic showing the h-BN/PEG treatment on leather for imparting mechanical reinforcement and thermal insulation properties.

are colloidal dispersions of micro- or nanosized particles.[16] Shear thickening occurs when viscosity increases with applied shear stress or shear rates. Under low shear rates, the viscosity will be less, whereas under high shear rates, viscosity increases due to hydrodynamic forces and particle cluster formation.[17] STFs are used in energy-damping devices[18] and impact and stab-resistant fabrics for body armors and protective wears.[19] Applying shear thickeners over fabrics provided higher absorption of impact energy.[20] A STF made of silica/ethylene glycol dispersion was used for developing stab-proof materials.[17] Glass-fiber-reinforced polymers impregnated with STF made of silica nanoparticles/PEG_{200} showed energy dissipation performance.[21]

Leather is obtained by the chemical treatment of animal skin and hides. It is a highly durable, flexible, soft material thereby mostly used in fabrics, bags, footwear, gloves, and upholstery. Nanoparticles are used in different stages of leather processing including tanning, retanning, dyeing, and post-tanning. The incorporation of nanoparticles within the leather matrix can improve the functional properties.[22] Modified silver nanoparticles were employed for leathers with durable antibacterial activity.[23] Multifunctional leathers with self-cleaning properties under visible light, bacterial-sensitive and fungi toxic properties were prepared by treating with Ag−N−TiO_2.[24] Our group has previously reported functional leathers including conducting leathers,[25] magnetic leathers,[26] and bifunctional leathers with both electric and magnetic properties.[22]

In this study, we synthesized h-BN nanoparticles via a modified single-step hydrothermal synthesis[7] and developed high-performance leathers after treating with the dispersion of h-BN in PEG_{200}. The synthesized h-BN nanoparticles and treated leathers were characterized by employing spectroscopic techniques, including surface and particle analysis. The treated leathers were studied for thermal insulation against heat and cold environments. The dampening and viscoelastic properties of the control as well as treated leathers were evaluated using dynamic mechanical analysis (DMA) to determine their potential for applications in absorption of energy.

EXPERIMENTAL SECTION

Materials. Boric acid and polyethylene glycol (molecular weight: 200) were purchased from Sigma-Aldrich, India. Urea was purchased from Sisco Research Laboratories Pvt. Ltd., India. Ammonia solution was purchased from Rankem Chemicals, India. White crust goat leathers were procured from a tannery in Chennai. All of the chemicals were of analytical grade and used without any further purification. Deionized distilled water was used throughout the experiments.

https://doi.org/10.1021/acsomega.2c05567
ACS Omega 2022, 7, 45120−45128

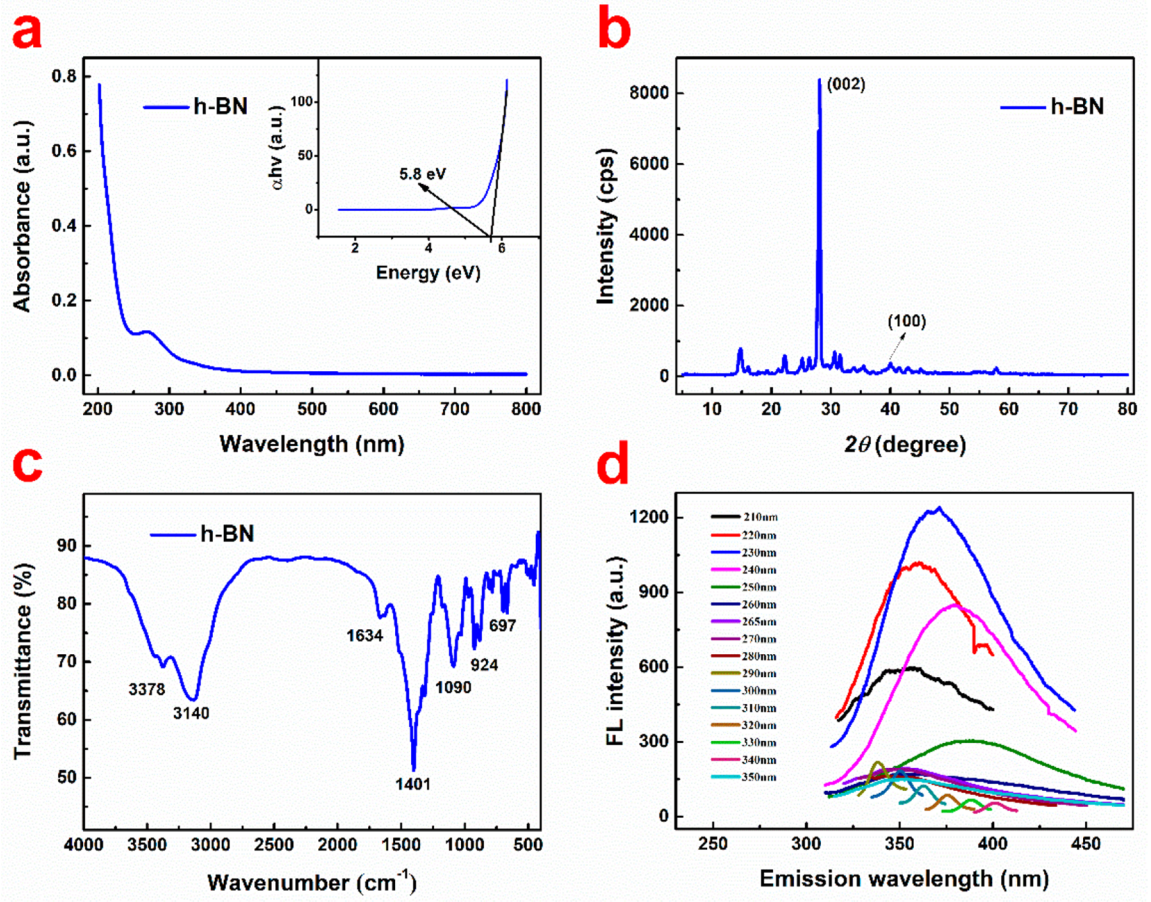

Figure 2. (a) UV−vis spectrum (inset: TAUC plot), (b) XRD data, (c) FT-IR spectrum, and (d) fluorescence spectrum of h-BN nanoparticles.

Synthesis of h-BN Nanoparticles. Following the bottom-up approach method, h-BN nanoparticles were synthesized via a facile single-step hydrothermal reaction reported previously with slight modification, using boric acid and urea as precursors (Figure 1a). Briefly, boric acid (1 g) was dissolved in ethanol (20 mL) and deionized water (10 mL). Subsequently, urea (2.94 g) dissolved in 10% liquid ammonia solution (20 mL) was added to the above solution. This mixture was transferred into a Teflon-lined stainless steel autoclave and heated hydrothermally at 200 °C for 12 h. The obtained h-BN nanoparticle dispersion was cooled to 30 °C and vacuum filtered through a 0.22 μm pore size filter paper and centrifuged at 14000 rpm for 45 min. The top supernatant containing h-BN nanoparticles was collected, freeze-dried, and stored for further studies.

Preparation of h-BN/PEG-Treated Leathers. Dispersions of PEG_{200} and h-BN nanoparticles were prepared at a concentration of 10 and 1 wt %, respectively (corresponding to the weight of leather), by ultrasonication for 5 min. White goat crust leathers were soaked overnight in distilled water for rewetting and then treated with the above dispersions by tumbling them in a rotating small drum for 2 h (Figure 1b). Treated leathers were air-dried at 30 °C.

Characterization of h-BN Nanoparticles and h-BN/PEG-Treated Leathers. The absorption of h-BN nanoparticles was recorded using a Shimadzu UV spectrophotometer (UV-1800) over the wavelength of 200−800 nm. Fourier transform infrared (FT-IR) spectroscopy of h-BN nanoparticles and h-BN/PEG-treated leathers was performed for the identification of functional groups using a PerkinElmer FT-IR spectrometer over the range of 4000−400 cm^{-1} at a resolution of 4 cm^{-1}. The crystal structure of h-BN nanoparticles was studied using a Rigaku Miniflex II X-ray diffractometer employing Cu Kα radiation with λ = 1.5406 Å in the 2θ range of 5 to 80°. The analysis was performed with a sampling rate of 4°/min and a step size of 0.02°. Photoluminescence studies were conducted using an F-7000 (HITACHI) fluorescence spectrophotometer at excitation wavelengths from 210 to 350 nm over the emission wavelength range of 300−500 nm. The structure and morphology of h-BN nanoparticles were characterized using field emission scanning electron microscopy (FESEM) (TESCAN Clara). Atomic force microscopy (AFM) was performed on an NTEGRA PRIMA (NT-MDT, Russia) equipped with a scanning probe for investigating the surface morphology of h-BN nanoparticles. The high-resolution transmission electron microscopy (HRTEM) was also performed on the h-BN nanoparticles using a JEOL 3010 instrument working at 100 kV. Leathers treated with h-BN nanoparticles and PEG_{200} were characterized using FESEM for surface and cross-sectional morphology. The distribution of elements over the surface and cross section of treated leathers was analyzed by elemental mapping with energy-dispersive X-ray (EDX) analysis. Heat insulation studies, according to standard IS 15298 (Part 1): 2011 and ISO 20344: 2004-512, were performed on leather using a PEGASIL (Portugal) instrument. Leather samples were fabricated into an envelope shape, and stainless steel balls were inserted and conditioned to a constant temperature of 23 ± 2

https://doi.org/10.1021/acsomega.2c05567
ACS Omega 2022, 7, 45120−45128

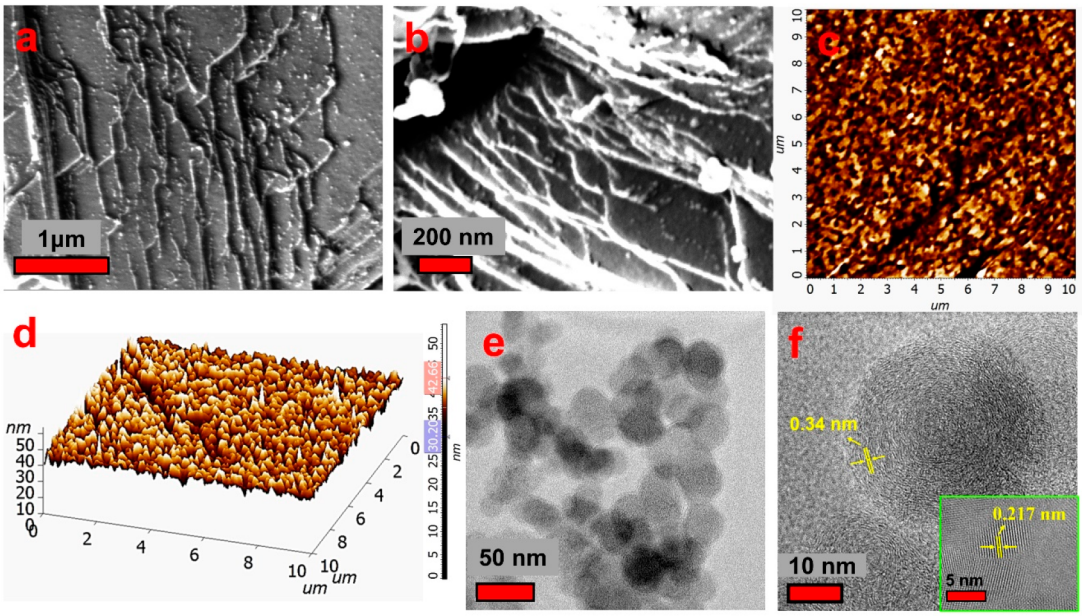

Figure 3. FESEM images of h-BN nanoparticles at (a) lower and (b) higher magnifications; AFM images of h-BN nanoparticles in (c) two-dimensional (2D) and (d) three-dimensional (3D) views; HRTEM images of h-BN nanoparticles at (e) low and (f) high magnification showing the lattice fringe corresponding to the (002) plane of h-BN (inset shows the lattice fringe corresponding to the (100) plane of h-BN).

°C and kept in a preheated sand bath over the hot plate at a temperature of 150 °C; the temperature inside the leather samples was recorded as a function of time, using stainless steel balls as a transfer medium, which was connected to the temperature sensor. The insulation against cold was determined by a PEGASIL (Portugal) instrument following IS 15298 (Part 1): 2011 and ISO 20344: 2004-513 standards. Leather samples were fabricated into an envelope shape, and stainless steel balls were inserted and further conditioned to a constant temperature of 23 ± 2 °C and placed in an insulated cold box of −17 ± 2 °C. The temperature inside the leather samples was recorded as a function of time using stainless steel balls as the transfer medium, which was connected to a temperature sensor. The viscoelastic properties of the leathers at different temperatures were evaluated using a DMA-6100 instrument by heating the sample from 25 to 150 °C at a rate of 3 °C/min and simultaneously measuring the dynamic mechanical properties under a tension mode at a frequency of 1 Hz. A low-velocity drop-weight impact resistance test for untreated and treated leathers against mechanical risks was conducted according to EN 13594:2015 6.9 with an impact energy of 5 J and drop striker mass of 2.5 kg. The test was also conducted for the composite obtained by stitching the leathers with lining and padding materials that are generally used to make leather gloves.

RESULTS AND DISCUSSION

Characterization of h-BN Nanoparticles. h-BN nanoparticles were synthesized via a facile single-step hydrothermal reaction reported previously. The formation of h-BN nanoparticles by hydrothermal synthesis was evaluated employing UV−visible spectroscopy (Figure 2a). The absorption spectrum of h-BN nanoparticles shows a broader peak with a maximum UV absorption near 200 nm corresponding to the increased band gap energy of nanoparticles due to the quantum confinement.[27] The Coulombic interaction in two-dimensional h-BN nanoparticles produces electron−hole pairs (excitons). The peak at 268 nm indicates the absorption by excitons in h-BN nanoparticles formed due to crystal defects.[28] The TAUC plot (inset of Figure 2a) displays the band gap energy value of about 5.8 eV, indicating the multilayered h-BN structures.[29]

X-ray diffraction (XRD) was employed to study the crystal structure and identify the crystalline phase of as-synthesized h-BN nanoparticles. The X-ray diffractogram shows a sharp diffraction peak at 28.1° corresponding to the 002 plane of the hexagonal crystal structure of the h-BN nanoparticles (Figure 2b). The average crystallite size calculated using Debye−Scherrer's equation is found to be 0.388 nm, whereas the *d*-spacing between the crystal planes in h-BN nanoparticles is around 0.32 nm. FT-IR spectra of the h-BN nanoparticles revealed the characteristic transmittance peaks at 3140 and 3378 cm^{-1} corresponding to the O−H and N−H stretching frequencies, respectively, which are due to the presence of surface groups over the nanoparticles (Figure 2c). The sharp transmittance peaks at 1401, 1090, and 1634 cm^{-1} are due to the B−N stretching mode of vibrations. The peak at 697 cm^{-1} denotes the B−N−B bending mode of vibrations. The photoluminescence of h-BN nanoparticles was studied over a range of UV excitation wavelengths from 210 to 350 nm. The emission spectra shown in Figure 2d revealed an increase in the emission intensity with an increase in UV excitation wavelength until λ_{exc} of 230 nm and then decreased drastically. Maximum fluorescence emission is observed at an excitation wavelength of 230 nm with UV emission near 370 nm. The sp^3 bonding between interlinked layers in boron nitride may be the origin for the broad emission spectrum.[30]

The micrographs of h-BN nanoparticles acquired from FESEM analysis exhibit sheet-like morphology for the as-synthesized h-BN nanoparticles (Figure 3a,b). Additional low-magnification FESEM images of the h-BN nanoparticles are provided in Figure S1, showing the individual particles and the layered structure. The surface morphology was also studied by AFM using tapping mode over h-BN nanoparticles coated on

https://doi.org/10.1021/acsomega.2c05567
ACS Omega 2022, 7, 45120−45128

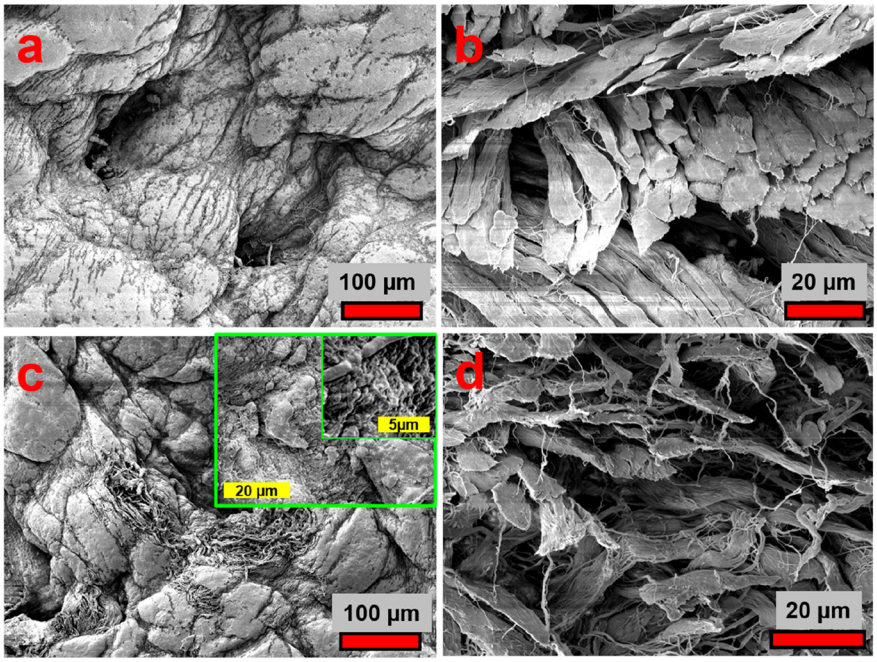

Figure 4. FESEM images of the (a) surface and (b) cross section of control leather and the (c) surface (insets show the presence of h-BN nanoparticles in magnified view) and (d) cross section of h-BN/PEG-treated leather.

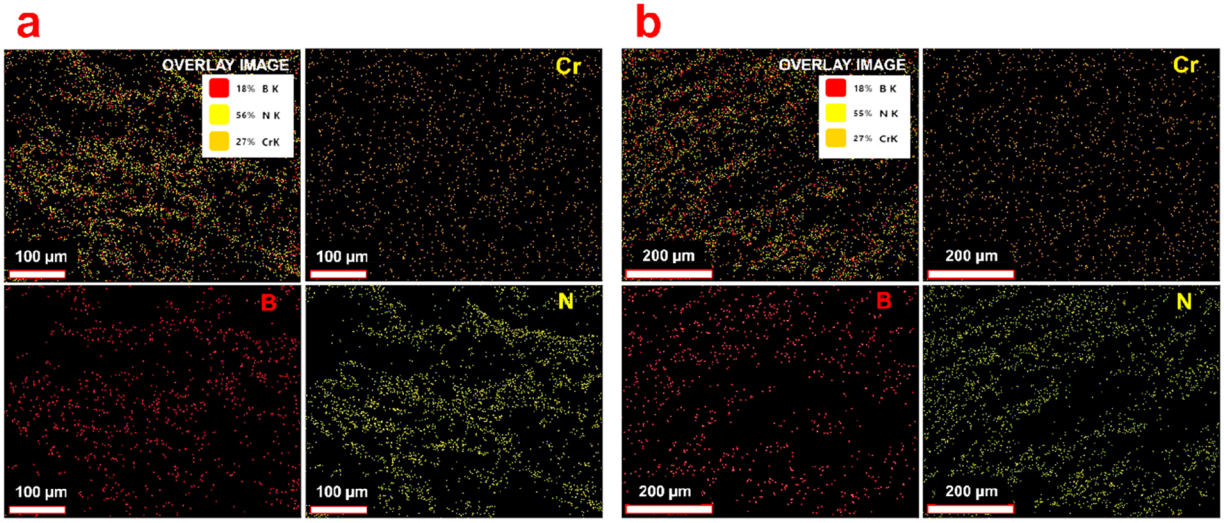

Figure 5. EDX elemental mapping of the cross-section of (a) control leather and (b) h-BN/PEG-treated leather showing the presence of boron, nitrogen, and chromium elements.

the glass surface. The particle size is approximately 30−43 nm, as observed in the two-dimensional surface view (Figure 3c), and the elevation is found to be less than 15 nm from the height profile observed in the three-dimensional view (Figure 3d). The HRTEM images display a particle size of 30−50 nm for the as-synthesized h-BN nanoparticles (Figure 3e), which is in accordance with the AFM results. HRTEM images show onion-like lattice fringes and at higher resolution displayed highly ordered and parallel fringes with a *d*-spacing of 0.34 and 0.217 nm, corresponding to the (002) and (100) planes of h-BN nanoparticles, respectively (Figure 3f). It indicates the good crystalline nature of boron nitride nanoparticles as previously reported.[31]

Characterization of h-BN/PEG-Treated Leather. The as-synthesized h-BN nanoparticles were dispersed in PEG_{200} and treated with white crust leathers. FESEM images of the treated leathers reveal the presence of h-BN nanoparticles on the grain surface in comparison to the untreated control leather (Figure 4a,c). The micrographs of the cross section of the control leathers displayed a compact fiber bundle, while the leather samples treated with h-BN nanoparticles exhibit a well-opened fiber structure (Figure 4b,d). This could be due to the lubricating effect of PEG. Additional low-magnification FESEM images of the control and h-BN/PEG-treated leathers are provided in Figure S2, showing the surface and the cross-sectional views.

Elemental mapping using EDX analysis of the cross sections of the control and h-BN/PEG-treated leathers is shown in Figure 5 and Figure S3. The analysis reveals the presence of elements such as boron, nitrogen, carbon, and chromium. The

https://doi.org/10.1021/acsomega.2c05567
ACS Omega 2022, 7, 45120−45128

presence of chromium is expected as the chrome-tanned leathers were employed in this study. The appearance of a carbon peak in the EDX spectra is also anticipated as the leathers comprise the collagen fibers. The significant presence of boron and nitrogen elements in the spectra asserted the successful incorporation of h-BN nanoparticles over the leathers. The presence of boron in control leather could be due to the impurities present in some of the chemicals used for processing leather. The FT-IR spectrum of the control and h-BN/PEG-treated leather is shown in Figure S4. The peaks at 1654, 1554, and 1238 cm^{-1} correspond to the amide I, II, and III groups of collagen, whereas the peaks at 3313 cm^{-1} correspond to the OH stretching and NH groups. A significant peak at 1089 cm^{-1} in treated leather indicates the B−N stretching frequency, implying the presence of h-BN nanoparticles.

Thermal Insulation Performance of h-BN/PEG-Treated Leather. The control and h-BN/PEG-treated leathers were investigated for heat insulation properties. Leather samples fabricated into an envelope shape were preconditioned to a constant temperature of 23 ± 2 °C and kept in a preheated sand bath over the hot plate at a temperature of 150 °C. Temperature changes inside the samples were measured using the temperature measuring device connected to the temperature probe and recorded as a function of time, which displayed the increase of temperature inside the leather samples. The observed temperature difference from the initial temperature for control leather is 30 °C and for h-BN/PEG-treated leather is 28.6 °C (Table S1). Thus, h-BN/PEG-treated leathers exhibited increased heat insulation compared to the control leather. The cold insulation studies were also conducted over the control and h-BN/PEG-treated samples by determining the temperature difference of leather samples. Leather samples were fabricated into an envelope shape and preconditioned to a constant temperature of 23 ± 2 °C and placed in a cold box regulated to the temperature of −17 ± 2 °C. Temperature changes inside the samples were measured using the temperature measuring device connected to the temperature probe and recorded as a function of time, which displayed the gradual decrease of the temperature inside the leather samples. As seen from Table S1, control leather displayed a temperature difference of 10.6 °C from the initial temperature, whereas the h-BN/PEG-treated leather showed a difference of 8.6 °C, making the latter an improved cold insulating material. Both heat and cold insulation studies on leathers revealed a significant increase in the thermal insulation properties of h-BN/PEG-treated leathers (Figure 6). Although the h-BN is a highly thermal conductive material, the dispersion of h-BN in PEG could have altered the thermal properties of the composite (h-BN/PEG) toward insulation behavior, which is reported herein for the first time. In addition, the h-BN/PEG-treated leathers displayed a well opened fiber structure compared to the control leathers, as seen in FESEM images (Figure 4). This implies that the h-BN/PEG-treated leathers are highly porous and expected to trap more amount of air. Air is one of the highly insulating materials, and it cannot effectively transfer the heat or cold when trapped in pores in small discontinuous cells. Hence, the h-BN/PEG-treated leathers with more interconnected pores display improved thermal insulation properties compared to the untreated control leathers, which is highly desirable for products such as gloves and garments that are used in very cold or hot environments.

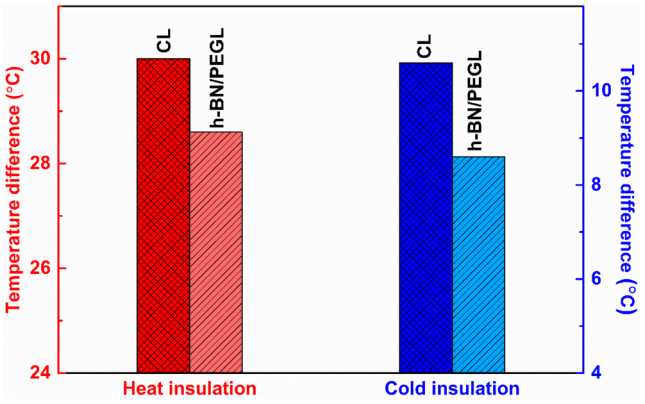

Figure 6. Temperature difference data from heat and cold insulation analysis of control leather and h-BN/PEG-treated leather.

Mechanical Property of h-BN/PEG-Treated Leather. The dampening and viscoelastic properties of the control and treated leather samples were measured using DMA at different temperatures. The transitions of dynamic properties of leathers with the increase in temperature correspond to the plateau of glass transition behavior. The leathers treated with PEG and h-BN/PEG exhibited a decrease in storage modulus, an increase and subsequent drop in loss modulus, and an increase in tan δ, indicating the changes in properties in the glass transition plateau (Figure S5). The control leathers exhibited an increase and consequent decrease in storage, loss modulus, and tan δ values (Figure S5a). The storage modulus reveals the ability of the material to store energy elastically. The changes in storage modulus with temperature for the control, PEG-treated, and h-BN/PEG-treated leathers are shown in Figure 7a. h-BN/PEG-treated leather possessed an initial storage modulus of 14.8 MPa, whereas the control and PEG-treated leather showed comparatively lower values of 3.6 and 8.3 MPa, respectively. A significant decrease in the storage modulus (E') was observed for leather samples with an increase in temperature from 25 to 150 °C. The tan δ, the ratio of loss to storage modulus, signifies the ability of the material to dissipate the energy. Figure 7b illustrates the change in tan δ with temperature. h-BN/PEG-treated leathers displayed a higher tan δ value of 0.10, while the control and PEG-treated leather showed lower tan δ values of 0.036 and 0.07, respectively. A higher tan δ value implies an enhanced dampening efficiency of h-BN/PEG-treated leathers, which could be due to the incorporation of shear thickening fluid comprising PEG and 2D-layered material such as h-BN nanoparticles. Overall high stress and strain values were observed for h-BN/PEG-treated leathers relative to control and PEG-treated leather and consistent with the other dynamic mechanical properties such as storage modulus and tan δ (Figure 7c,d). Acrylic/montmorillonite nanocomposites were used in leather finishing for improving the physical and mechanical properties, whereas waterborne polyhexamethylene guanidine-embedded polyurethane was coated on leather fibers to obtain a composite with good durability, wet management, and temperature-adaptive flexibility.[32,33] It can be seen that the dynamic mechanical properties of our h-BN/PEG-treated leathers are comparable or even better than those from the previously reported results.

From the DMA data, it is evident that h-BN/PEG-treated leathers have potential for applications in the absorption of energy due to higher storage modulus and tan δ values. For example, the leathers used in gloves, shoes, and garments in

https://doi.org/10.1021/acsomega.2c05567
ACS Omega 2022, 7, 45120−45128

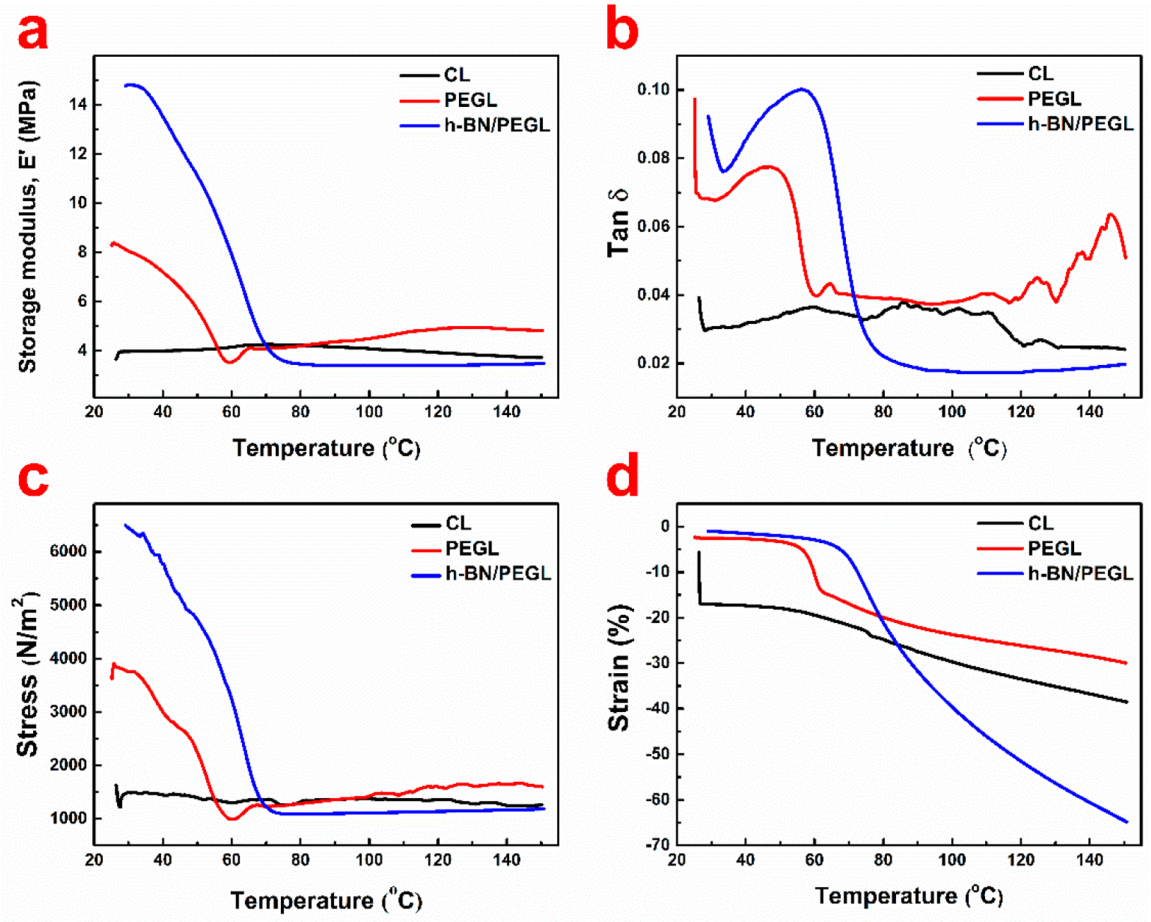

Figure 7. DMA analysis of the control, PEG-treated, and h-BN/PEG-treated leather. (a) Storage modulus (E'), (b) tan δ, (c) stress, and (d) % strain as a function of temperature.

strategic sectors such as the army are expected to have high impact resistance owing to the possible impact from various objects. Hence, the developed h-BN/PEG-treated leathers could be used in the aforementioned applications.

The impact resistance of control and h-BN/PEG-treated leathers (thickness: 1 ± 0.1 mm) was evaluated by measuring the mean transmitted force against an impact, using a low-velocity drop-weight test. Table S2 shows the mean transmitted force upon the impact energy of 5 J, and the results showed an improved impact resistance for h-BN/PEG-coated leather compared to that of untreated control leather. Nevertheless, the obtained results were not meeting the requirements of the EN 13594:2015 6.9 standard since the test is normally conducted for the whole glove rather than leather alone. Hence, the control and h-BN/PEG-treated leathers were stitched with lining and padding materials, which are generally used to make leather gloves, and made into a composite (thickness: 3 ± 0.1 mm) and further tested. The results show that the leather composites exhibited a substantial reduction in the mean transmitted force compared to the bare leather as envisaged, providing more impact resistance owing to the insertion of lining and padding materials (Table S3). Leather composite made of h-BN/PEG leather displayed improved impact resistance relative to control leather. Nevertheless, further studies on fine-tuning of the treatment as well as testing of the whole glove made of treated leathers need to be carried out in order to meet the requirements of the standard.

CONCLUSIONS

The two-dimensional nanomaterial, h-BN, was successfully synthesized by the modified hydrothermal method. The as-synthesized h-BN nanoparticles, characterized using AFM and HRTEM, possessed a particle size of 30−50 nm, and the optical properties were studied using UV and fluorescence spectrometer. The white crust leather samples treated with the purified h-BN along with PEG_{200} were characterized using FESEM/EDX and FT-IR. Heat insulation studies investigated after measuring the increase in temperature after placing samples in a preheated sand bath over the hot plate at 150 °C, displayed a temperature difference of 30 °C for control leather and 28.6 °C for h-BN/PEG-treated leather. The insulation against cold was studied by measuring the decrease in temperature after placing samples in an insulated cold box, exhibiting a temperature difference of 10.6 °C for control leather and 8.6 °C for h-BN/PEG-treated leather. Consequently, the h-BN/PEG-treated leathers exhibited improved thermal insulation compared to the control leather. The h-BN/PEG-treated leathers display robust improvement in the dampening and viscoelastic properties, primarily storage modulus and tan δ, as revealed through the dynamic mechanical analysis. The leather composites comprising h-BN/PEG exhibited improved impact resistance, as confirmed by a low-velocity drop-weight test. The results demonstrate that the h-BN/PEG-treated leathers could be utilized for

https://doi.org/10.1021/acsomega.2c05567
ACS Omega 2022, 7, 45120−45128

strategic product applications demanding properties such as high impact resistance and thermal insulation.

■ ASSOCIATED CONTENT

Supporting Information

The Supporting Information is available free of charge at https://pubs.acs.org/doi/10.1021/acsomega.2c05567.

FESEM images of h-BN nanoparticles; FESEM images and sum spectrum for elemental analysis of surface and cross section of control and h-BN/PEG-treated leather; changes in the storage modulus (E'), loss modulus (E''), and tan δ with increase in temperature for control, PEG-treated, and h-BN/PEG-treated leather; FT-IR spectrum, heat, and cold insulation studies of control leather and h-BN/PEG-treated leather; impact resistance test of leathers and leather composites of control and h-BN/PEG-treated leathers (PDF)

■ AUTHOR INFORMATION

Corresponding Author

Thanikaivelan Palanisamy − *Advanced Materials Laboratory, Council of Scientific and Industrial Research (CSIR)-Central Leather Research Institute (CLRI), Chennai 600020, India; Academy of Scientific and Innovative Research (AcSIR), Ghaziabad 201002, India;* orcid.org/0000-0003-0823-6117; Phone: +91 44 24437142; Email: thanik8@yahoo.com, thanik@clri.res.in

Authors

Arya P Bhasi − *Advanced Materials Laboratory, Council of Scientific and Industrial Research (CSIR)-Central Leather Research Institute (CLRI), Chennai 600020, India; Academy of Scientific and Innovative Research (AcSIR), Ghaziabad 201002, India;* orcid.org/0000-0003-0106-0825

Nithiya Hanna Wilson − *Advanced Materials Laboratory, Council of Scientific and Industrial Research (CSIR)-Central Leather Research Institute (CLRI), Chennai 600020, India;* orcid.org/0000-0001-5476-5031

Complete contact information is available at: https://pubs.acs.org/10.1021/acsomega.2c05567

Author Contributions

Arya P Bhasi: Methodology, data curation, writing-original draft preparation, reviewing and editing. Nithiya Hanna Wilson: Methodology, reviewing, and editing. Thanikaivelan Palanisamy: Conceptualization, supervision, writing, reviewing and editing, funding acquisition. All authors have approved the final version of the manuscript.

Notes

The authors declare no competing financial interest.

■ ACKNOWLEDGMENTS

The authors thank the CSIR, New Delhi, for financial support under the CHILLS Project (MLP 2005). The authors thank CLRI-CATERS for the XRD, heat and cold insulation, and FESEM facilities, and Prof. T. Pradeep, Nano Facilities, IIT Madras, for the HRTEM facility. CSIR-CLRI Communication No. 1735.

■ REFERENCES

(1) Chen, P.; Zhang, Z.; Duan, X.; Duan, X. Chemical synthesis of two-dimensional atomic crystals, heterostructures and superlattices. *Chem. Soc. Rev.* **2018**, *47* (9), 3129−3151.

(2) Liu, C.; Xu, K.; Shi, Y.; Wang, J.; Ma, S.; Feng, Y.; Lv, Y.; Yang, F.; Liu, M.; Song, P. Fire-Safe, Mechanically Strong and Tough Thermoplastic Polyurethane/MXene Nanocomposites with Exceptional Smoke Suppression. *Mater. Today Phys.* **2022**, *22*, 100607.

(3) Yang, L.; Wang, D.; Liu, M.; Liu, H.; Tan, J.; Wang, Z.; Zhou, H.; Yu, Q.; Wang, J.; Lin, J.; Zou, X.; Qiu, L.; Cheng, H.-M.; Liu, B. Glue-Assisted Grinding Exfoliation of Large-Size 2D Materials for Insulating Thermal Conduction and Large-Current-Density Hydrogen Evolution. *Mater. Today* **2021**, *51*, 145−154.

(4) Han, G.; Zhao, X.; Feng, Y.; Ma, J.; Zhou, K.; Shi, Y.; Liu, C.; Xie, X. Highly flame-retardant epoxy-based thermal conductive composites with functionalized boron nitride nanosheets exfoliated by one-step ball milling. *Chem. Eng. J.* **2021**, *407*, 127099.

(5) Kainthola, A.; Bijalwan, K.; Negi, S.; Sharma, H.; Dwivedi, C. Hydrothermal synthesis of highly stable boron nitride nanoparticles. *Mater. Today: Proc.* **2020**, *28*, 138−140.

(6) Jiang, X. F.; Weng, Q.; Wang, X. B.; Li, X.; Zhang, J.; Golberg, D.; Bando, Y. Recent progress on fabrications and applications of boron nitride nanomaterials: a review. *J. Mater. Sci. Technol.* **2015**, *31* (6), 589−598.

(7) Jerome, R.; Sundramoorthy, A. K. Hydrothermal synthesis of boron nitride quantum dots/poly (luminol) nanocomposite for selective detection of ascorbic acid. *J. Electrochem. Soc.* **2019**, *166* (9), B3017.

(8) Kumar, V.; Nikhil, K.; Roy, P.; Lahiri, D.; Lahiri, I. Emergence of fluorescence in boron nitride nanoflakes and its application in bioimaging. *RSC Adv.* **2016**, *6* (53), 48025−48032.

(9) Hou, J.; Li, G.; Yang, N.; Qin, L.; Grami, M. E.; Zhang, Q.; Wang, N.; Qu, X. Preparation and characterization of surface modified boron nitride epoxy composites with enhanced thermal conductivity. *RSC Adv.* **2014**, *4* (83), 44282−44290.

(10) Li, H.; Tay, R. Y.; Tsang, S. H.; Zhen, X.; Teo, E. H. T. Controllable synthesis of highly luminescent boron nitride quantum dots. *Small* **2015**, *11* (48), 6491−6499.

(11) Li, J.; Majety, S.; Dahal, R.; Zhao, W.; Lin, J.; Jiang, H. Dielectric strength, optical absorption, and deep ultraviolet detectors of hexagonal boron nitride epilayers. *Appl. Phys. Lett.* **2012**, *101* (17), 171112.

(12) Liu, Z.; Gong, Y.; Zhou, W.; Ma, L.; Yu, J.; Idrobo, J. C.; Jung, J.; MacDonald, A. H.; Vajtai, R.; Lou, J.; Ajayan, P. M. Ultrathin high-temperature oxidation-resistant coatings of hexagonal boron nitride. *Nat. Commun.* **2013**, *4* (1), 2541.

(13) Terao, T.; Zhi, C.; Bando, Y.; Mitome, M.; Tang, C.; Golberg, D. Alignment of boron nitride nanotubes in polymeric composite films for thermal conductivity improvement. *J. Phys. Chem. C* **2010**, *114* (10), 4340−4344.

(14) Huo, B.; Liu, B.; Chen, T.; Cui, L.; Xu, G.; Liu, M.; Liu, J. One-step synthesis of fluorescent boron nitride quantum dots via a hydrothermal strategy using melamine as nitrogen source for the detection of ferric ions. *Langmuir* **2017**, *33* (40), 10673−10678.

(15) Lee, G. J.; Lee, M. K.; Park, J. J.; Hyeon, D. Y.; Jeong, C. K.; Park, K. I. Piezoelectric energy harvesting from two-dimensional boron nitride nanoflakes. *ACS Appl. Mater. Interfaces* **2019**, *11* (41), 37920−37926.

(16) Zarei, M.; Aalaie, J. Application of shear thickening fluids in material development. *J. Mater. Res. Technol.* **2020**, *9* (5), 10411−10433.

(17) Kang, T. J.; Hong, K. H.; Yoo, M. R. Preparation and properties of fumed silica/Kevlar composite fabrics for application of stab resistant material. *Fibers Polym.* **2010**, *11* (5), 719−724.

(18) Tan, Z.; Ma, H.; Zhou, H.; Han, X.; Cho, C. The influence of graphene on the dynamic mechanical behaviour of shear thickening fluids. *Adv. Powder Technol.* **2019**, *30* (10), 2416−2421.

(19) Zhao, C.; Gong, X.; Wang, S.; Jiang, W.; Xuan, S. Shear stiffening gels for intelligent anti-impact applications. *Cell Rep. Phys. Sci.* **2020**, *1* (12), 100266.
(20) Majumdar, A.; Laha, A.; Bhattacharjee, D.; Biswas, I. Tuning the structure of 3D woven aramid fabrics reinforced with shear thickening fluid for developing soft body armour. *Compos. Struct.* **2017**, *178*, 415−425.
(21) Sun, L.; Wei, M.; Zhu, J. Low velocity impact performance of fiber-reinforced polymer impregnated with shear thickening fluid. *Polym. Test.* **2021**, *96*, 107095.
(22) Wilson, N. H.; Ragothaman, M.; Palanisamy, T. Bimetallic Copper−Iron Oxide Nanoparticle-Coated Leathers for Lighting Applications. *ACS Appl. Nano Mater.* **2021**, *4* (4), 4055−4069.
(23) Sportelli, M. C.; Picca, R. A.; Paladini, F.; Mangone, A.; Giannossa, L. C.; Di Franco, C.; Gallo, A. L.; Valentini, A.; Sannino, A.; Pollini, M.; Cioffi, N. Spectroscopic characterization and nanosafety of Ag-modified antibacterial leather and leatherette. *Nanomaterials* **2017**, *7* (8), 203.
(24) Gaidau, C.; Petica, A.; Ignat, M.; Iordache, O.; Ditu, L. M.; Ionescu, M. Enhanced photocatalysts based on Ag-TiO_2 and Ag-N-TiO_2 nanoparticles for multifunctional leather surface coating. *Open Chem.* **2016**, *14* (1), 383−392.
(25) Wegene, J. D.; Thanikaivelan, P. Conducting leathers for smart product applications. *Ind. Eng. Chem. Res.* **2014**, *53* (47), 18209−18215.
(26) Thanikaivelan, P.; Murali, R.; Krishnaraj, K. Magnetic leathers. *RSC Adv.* **2016**, *6* (8), 6496−6503.
(27) Stagi, L.; Ren, J.; Innocenzi, P. From 2-D to 0-D boron nitride materials, the next challenge. *Materials* **2019**, *12* (23), 3905.
(28) Lee, C. H.; Wang, J.; Kayatsha, V. K.; Huang, J. Y.; Yap, Y. K. Effective growth of boron nitride nanotubes by thermal chemical vapor deposition. *Nanotechnology* **2008**, *19* (45), 455605.
(29) Ikram, M.; Wakeel, M.; Hassan, J.; Haider, A.; Naz, S.; Ul-Hamid, A.; Haider, J.; Ali, S.; Goumri-Said, S.; Kanoun, M. B. Impact of Bi doping into boron nitride nanosheets on electronic and optical properties using theoretical calculations and experiments. *Nanoscale Res. Lett.* **2021**, *16* (1), 82.
(30) Tang, C.; Bando, Y.; Zhi, C.; Golberg, D. Boron−oxygen luminescence centres in boron−nitrogen systems. *Chem. Commun.* **2007**, No. 44, 4599−4601.
(31) Lei, Z.; Xu, S.; Wan, J.; Wu, P. Facile preparation and multifunctional applications of boron nitride quantum dots. *Nanoscale* **2015**, *7* (45), 18902−18907.
(32) Bondaryeva, A.; Mokrousova, O. The Acrylic/Montmorillonite Nanocomposites for Leather Finishing. In *Proceedings of the 8th International Conference on Advanced Materials and Systems*; INCDTP - Leather and Footwear Research Institute (ICPI): Bucharest, Romania, 2020; pp 43−48.
(33) Gong, D.; Han, Y.; Zhang, Q.; Xu, B.; Zhang, C.; Li, K.; Tan, L. Development of Leather Fiber/Polyurethane Composite with Antibacterial, Wet Management, and Temperature-Adaptive Flexibility for Foot Care. *ACS Biomater. Sci. Eng.* **2022**, *8* (10), 4557−4565.

https://doi.org/10.1021/acsomega.2c05567
ACS Omega 2022, 7, 45120−45128